JOURNAL OF THE AMERICAN CHEMICAL SOCIETY

Communication

pubs.acs.org/JACS

# Mesoscopic $CH_3NH_3PbI_3/TiO_2$ Heterojunction Solar Cells

Lioz Etgar,*[†,§] Peng Gao,[†] Zhaosheng Xue,[‡] Qin Peng,[†] Aravind Kumar Chandiran,[†] Bin Liu,[‡] Md. K. Nazeeruddin,[†] and Michael Grätzel[†]

[†]Laboratoire de Photonique et Interfaces, Institut des Sciences et Ingénierie Chimiques, École Polytechnique Fédérale de Lausanne, Switzerland

[‡]Department of Chemical and Biomolecular Engineering, National University of Singapore, Singapore

[§]Institute of Chemistry, The Hebrew University of Jerusalem, Jerusalem 91904, Israel

**ABSTRACT:** We report for the first time on a hole conductor-free mesoscopic methylammonium lead iodide ($CH_3NH_3PbI_3$) perovskite/$TiO_2$ heterojunction solar cell, produced by deposition of perovskite nanoparticles from a solution of $CH_3NH_3I$ and $PbI_2$ in $\gamma$-butyrolactone on a 400 nm thick film of $TiO_2$ (anatase) nanosheets exposing (001) facets. A gold film was evaporated on top of the $CH_3NH_3PbI_3$ as a back contact. Importantly, the $CH_3NH_3PbI_3$ nanoparticles assume here simultaneously the roles of both light harvester and hole conductor, rendering superfluous the use of an additional hole transporting material. The simple mesoscopic $CH_3NH_3PbI_3/TiO_2$ heterojunction solar cell shows impressive photovoltaic performance, with short-circuit photocurrent $J_{sc}$= 16.1 mA/cm$^2$, open-circuit photovoltage $V_{oc}$ = 0.631 V, and a fill factor FF = 0.57, corresponding to a light to electric power conversion efficiency (PCE) of 5.5% under standard AM 1.5 solar light of 1000 W/m$^2$ intensity. At a lower light intensity of 100W/m$^2$, a PCE of 7.3% was measured. The advent of such simple solution-processed mesoscopic heterojunction solar cells paves the way to realize low-cost, high-efficiency solar cells.

Due to their large optical cross section, nanocrystalline pigments are attractive light harvesters in solar conversion systems. In particular quantum dots (QDs) have attracted a lot of attention due to their tunable band gap.[1−3]A variety of strategies have been applied to integrate QDs into solar cells, including QD-polymer hybrid solar cells, QD-Schottky barrier solar cells, QD-sensitized titanium dioxide ($TiO_2$) solar cells, and QD hybrid bilayer solar cells.[4−12] Recent investigations have focused on depleted heterojunction devices, employing a mesoscopic wide band gap semiconductor oxide such as $TiO_2$ or ZnO as a thin spacer layer between the QDs and the conducting transparent oxide current collector.[13−21] Efficiencies of 5−6% were observed with these simple structures. In addition, a tandem QDs solar cell with the same structure has been demonstrated.[18] Multiple exciton generation (MEG) was also witnessed in a similar QDs based solar cell structure.[22,23] While such heterojunction QD solar cells show promising photovoltaic performance, they still face problems such as low stability, low open-circuit voltage, and fast carrier recombination which prevent them from achieving higher efficiencies.

The direct band gap, large absorption coefficient,[24,25] and high carrier mobility[26,27]of organo-lead halide perovskites render them very attractive for use as light harvesters in mesoscopic heterojunction solar cells. Their electronic properties can be tailored, allowing for, e.g., layered materials to be formed by controlling the distance and the electronic coupling between the inorganic sheets according to the structure of the organic component employed. The layered perovskites have high stability in dry air.

These perovskite nanopigments are notably easy to prepare and to deposit by simple solution processing via spin- or dip-coating. The perovskite precipitates from a solution of $PbI_2$ and methylammonium iodide, forming $CH_3NH_3PbI_3$ crystals within the pores and on the surface of the mesoscopic $TiO_2$ substrate. The ionic and covalent interaction between the metal cations and the halogen anions creates inorganic octahedra, while the cationic alkylammonium head groups provide charge balance to the structure. Previous reports used $CH_3NH_3PbI_3$ nanocrystals as sensitizers in photoelectrochemical cells with liquid electrolyte.[28−30] However, the performance of these systems rapidly declined due to dissolution of the perovskite. This problem was alleviated by replacing the electrolyte with a solid-state organic hole conductor.[31] Very recently, the tin iodide based perovskite $CsSnI_3$ has been employed as a hole conductor together with N719 as sensitizer in solid-state dye-sensitized solar cells, yielding a power conversion efficiency (PCE) of 8.5%.[32]

Here we report on a $CH_3NH_3PbI_3$ perovskite/$TiO_2$ heterojunction solar cell using anatase nanosheets with dominant (001) facets as the electron collector. The pervoskite acts as an absorber and at the same time as a hole conductor, rendering superfluous the use of an additional p-type material for transporting positive charge carriers. This simple mesoscopic heterojunction solar cell achieved a remarkable photovoltaic performance, with short-circuit photocurrent ($J_{sc}$) of 16.1 mA cm$^{-2}$, a fill factor (FF) of 0.57, and open-circuit voltage ($V_{oc}$) of 0.631 V, corresponding to a light to electric PCE of 5.5% under 1 sun intensity. This is the first report on the successful use of $CH_3NH_3PbI_3$ simultaneously as an absorber and hole-transporting material in a heterojunction solar cell.

The synthesis of $CH_3NH_3PbI_3$ and deposition on the mesoporous $TiO_2$ film was carried out by spin-coating of a 40 wt% precursor solution of $CH_3NH_3I$ and $PbI_2$ in $\gamma$-butyrolactone. Upon drying at room temperature, the film

**Received:** August 6, 2012
**Published:** October 8, 2012

dx.doi.org/10.1021/ja307789s | J. Am. Chem. Soc. 2012, 134, 17396−17399

coated onto the $TiO_2$ darkened in color, indicating the formation of $CH_3NH_3PbI_3$ in the solid state, confirmed by X-ray diffraction (XRD) spectroscopy (see Figure 2C).

Figure 1 presents a scheme of the device structure and its energy level diagram. The conduction and valence bands of the $CH_3NH_3PbI_3$ permit electron injection into the $TiO_2$ and hole transport to the gold back contact, respectively. The bottom section of the device acts as an electron collector and is composed of a 100 nm thick hole-blocking compact $TiO_2$ film deposited onto the FTO transparent glass front contact, followed by deposition of a ca. 500 nm thick layer of the $TiO_2$ nanosheets. The light is absorbed by the $CH_3NH_3PbI_3$ nanoparticles, which were deposited onto the $TiO_2$ by the spin-coating technique. A gold contact was evaporated on top of the $CH_3NH_3PbI_3$ thin film.

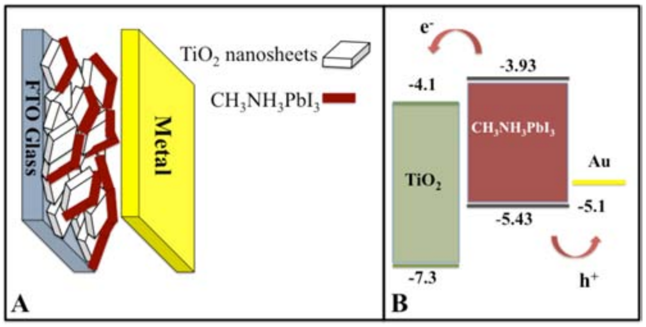

**Figure 1.** (A) Scheme of the device structure. (B) Energy level diagram of the $CH_3NH_3PbI_3/TiO_2$ heterojunction solar cell.

Figure 2D shows a typical XRD pattern of $TiO_2$ nanosheets synthesized at 180 °C. All the diffraction peaks are indexed to the anatase phase of $TiO_2$ (JCPDS No. 21-1272), indicating that the obtained product is pure anatase $TiO_2$. Figure 2A,B shows high-resolution scaning electron microscopy (HR-SEM) images of the cross section of the solar cell and the $TiO_2$ film, respectively. The change in contrast in Figure 2A above the compact $TiO_2$ layer indicates penetration of the $CH_3NH_3PbI_3$ nanocrystals into the pores within the anatase nanosheet film. Figure 2C shows XRD patterns of the $CH_3NH_3PbI_3$ on $TiO_2$ and on microscope glass. The peaks of $CH_3NH_3PbI_3$ on the microscope slide match closely with those of $CH_3NH_3PbI_3$ on $TiO_2$.

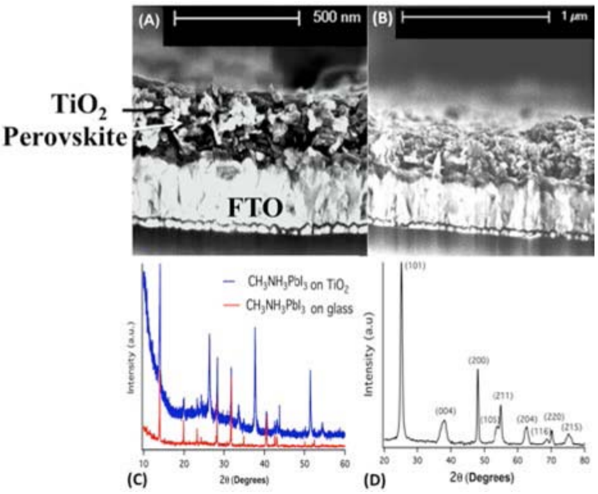

**Figure 2.** (A) High-resolution scanning electron microscopy (HR-SEM) picture of the cross section of the $CH_3NH_3PbI_3/TiO_2$ heterojunction solar cell. The dark areas can be attributed to the $CH_3NH_3PbI_3$ which penetrates into the mesoporous $TiO_2$ film. (B) HR-SEM of the cross section of the $TiO_2$ nanosheets film alone. (C) XRD pattern of the $CH_3NH_3PbI_3$ deposited on a $TiO_2$ nanosheet. (D) XRD pattern of an individual $TiO_2$ nanosheet.

Figure 3A exhibits *J*−*V* characteristics of the mesoscopic $CH_3NH_3PbI_3/TiO_2$ heterojunction photovoltaic cell under 1 sun illumination. Under standard reporting conditions, i.e., AM 1.5 solar light at 1000 W/m$^2$, the device produced $V_{oc}$ = 0.631 V and $J_{sc}$ = 16.1 mA cm$^{-2}$, with FF = 57%, corresponding to a PCE of 5.5% (Table 1). The PCE increases at 100 W/m$^2$ intensity to 7.28% with $J_{sc}$ = 2.14 mA cm$^{-2}$, FF = 62%, and $V_{oc}$ = 0.565 V.

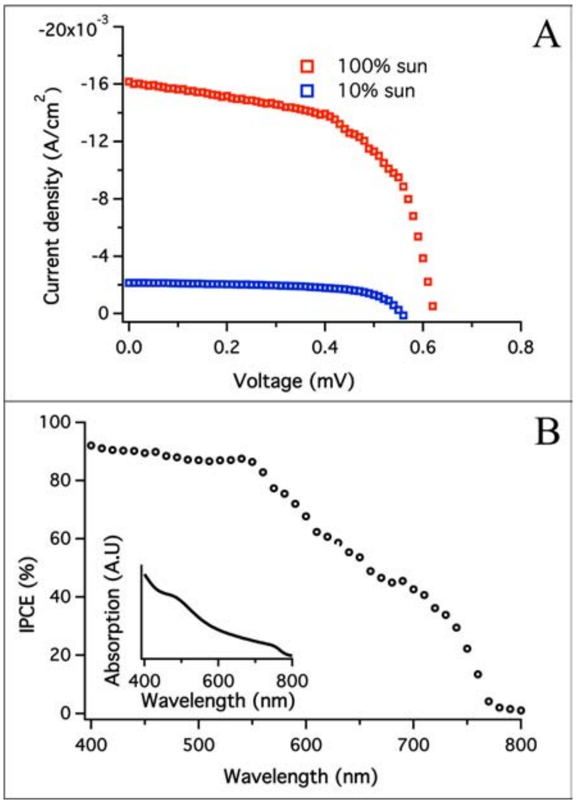

**Figure 3.** (A) *J*−*V* characteristic of the lead iodide perovskite/$TiO_2$ mesoscopic heterojunction solar cell. (B) IPCE spectrum of the device. Inset: absorption spectra of the perovskite layer on the $TiO_2$.

**Table 1. Photovoltaic Device Parameters of the $CH_3NH_3PbI_3/TiO_2$ Solar Cell**

| sun intensity | $J_{sc}$ (mA/cm$^2$) | $V_{oc}$ (mV) | FF | PCE (%) |
|---|---|---|---|---|
| 10 | 2.1 | 565.8 | 0.62 | 7.28 |
| 100 | 16.1 | 631.6 | 0.57 | 5.5 |

The incident photon to current conversion efficiency (IPCE) specifies the ratio of extracted electrons to incident photons at a given wavelength. The IPCE spectrum (Figure 3B) is plotted as a function of wavelength of the impinging light. The solid-state $CH_3NH_3PbI_3/TiO_2$ heterojunction solar cell shows an excellent photocurrent response from 400 to 800 nm, with the IPCE reaching a maximum of 90% in the wavelength range of 400−540 nm and decreasing at longer wavelengths until 800 nm. Integration of the IPCE spectrum over the AM1.5 solar emission yields a photocurrent density of 16.2 mA/cm$^2$, in reasonable agreement with the measured values. The inset of Figure 3B shows the absorption spectrum of the perovskite on the $TiO_2$ film.

It is important to note the that same cells made from standardly used $TiO_2$ nanoparticles (i.e., 101 exposed facets and 20 nm particles) achieved a PCE of only 2.8% at 1 sun intensity. This PCE is lower than that achieved using 001 $TiO_2$ nanosheets. As was discussed in our previous work,[20] the improved photovoltaic performance of the nanosheets compared to nanoparticulate films may be attributed to the higher concentration of ionic charge of the exposed (001) faces compared to the (101) facets, thus strengthening the attachment of the QDs to the $TiO_2$ surface and screening the electrons injected in the conduction band of the oxide.

In summary, the present work establishes for the first time that $CH_3NH_3PbI_3$ nanocrystals can act both as an efficient light harvester and as a hole transporter in solar cells comprising a meoscocopic $CH_3NH_3PbI_3/TiO_2$ heterojuntion. The role of the $TiO_2$ nanoplatelets is to accept electrons and transport them to the front collector. This eliminates the need to employ an additional organic or inorganic hole conductor, whose infiltration in the mesoporous $TiO_2$ has often posed difficulties in the past. There remains room for further very substantial improvement of the PCE, in particular by augmentation of the FF and $V_{oc}$ through control of the layer's crystallinity. This will be the focus of our continuing investigations. The fact that the perovskite is stable in dry ambient air and can be deposited by low-cost solution processing opens up new avenues for future development of high-efficiency, low-cost photovoltaic cells.

**$CH_3NH_3I$ Synthesis.** $CH_3NH_3I$ was synthesized by reacting 30 mL of methylamine (40% in methanol, TCI) and 32.3 mL of hydroiodic acid (57 wt% in water, Aldrich) in a 250 mL round-bottom flask at 0 °C for 2 h with stirring. The precipitate was recovered by putting the solution on a rotary evaporator and carefully removing the solvents at 50 °C. The yellowish raw product methylammonium iodide ($CH_3NH_3I$) was washed with diethyl ether by stirring the solution for 30 min, a step which was repeated three times, and then finally recrystallized from a mixed solvent of diethyl ether and ethanol. After filtration, the solid was collected and dried at 60 °C in a vacuum oven for 24 h.

**Synthesis and Purification of $TiO_2$ Nanosheets.** Synthesis of the nanosheets followed the typical experimental procedure.[33] A $Ti(OBu)_4$ (10 mL, 98%) and hydrofluoric acid (0.8 mL, 47%) solution was mixed in a 150 mL dried Teflon autoclave which was kept at 180 °C for 24 h, yielding well-defined rectangular sheet-like structures with a side length of 30 nm and a thickness of 7 nm. After reaction the dispersion was cooled to room temperature, and the white powder was separated by high-speed centrifugation and washed with ethanol, followed by several distilled water washings.

***Caution:** Hydrofluoric acid is extremely corrosive and a contact poison; it should be handled with extreme care! Hydrofluoric acid solution is stored in Teflon containers for use.*

The crystallographic properties of the perovskite structures deposited on FTO-$TiO_2$ and a microscopic slide were investigated using XRD with a Bruker D8 Discover apparatus. The instrument was set in "locked coupled" mode, and the acquisition was done in $\theta$−$2\theta$ mode for every 0.1° increment over the Bragg angle range of 10−60°.

**Solar Cell Fabrication.** Thin, dense $TiO_2$ layers of ∼100 nm thickness were deposited onto a $SnO_2$:F conducting glass substrate (15 Ω/cm, Pilkington) by the spray pyrolysis method.[34] The deposition temperature of the $TiO_2$ compact layer was 450 °C. $TiO_2$ nanosheet films of ∼0.5 μm thickness were spin-coated onto this substrate, using the $TiO_2$ nanosheets with 001 dominant facets. The $TiO_2$ layer was annealed at 500 °C for 30 min in air. The substrate was immersed in 40 mM $TiCl_4$ aqueous solutions for 30 min at 70 °C and washed with distilled water and ethanol, followed by annealing at 500 °C for 30 min in air.

The synthesis of $CH_3NH_3PbI_3$ on the $TiO_2$ surface was carried out by dropping a 40 wt% precursor solution of equimolar $CH_3NH_3I$ and $PbI_2$ in γ-butyrolactone onto the $TiO_2$ film. Film formation was induced by spin-coating (2000 rpm, 30 s) under glovebox conditions.

The film coated on the $TiO_2$ changed color upon drying at room temperature, indicating the formation of $CH_3NH_3PbI_3$ in the solid state. The $CH_3NH_3PbI_3$ film was annealed under argon for 15 min at 100 °C.

Finally the counter electrode was deposited by thermal evaporation of gold under a pressure of $5 \times 10^{-5}$ Torr. The active area was 0.12 cm$^2$. After the preparation, the cells were allowed to be exposed to air.

**Photovoltaic Characterization.** Photovoltaic measurements employed an AM 1.5 solar simulator equipped with a 450 W xenon lamp (model 81172, Oriel). Its power output was adjusted to match AM 1.5 global sunlight (100 mW/cm$^2$) by using a reference Si photodiode equipped with an IR-cutoff filter (KG-3, Schott) in order to reduce the mismatch between the simulated light and AM 1.5 (in the region of 350−750 nm) to less than 2%, with measurements verified at two PV calibration laboratories [ISE (Germany) and NREL (USA)]. $I$−$V$ curves were obtained by applying an external bias to the cell and measuring the generated photocurrent with a Keithley model 2400 digital source meter. The voltage step and delay time of photocurrent were 10 mV and 40 ms, respectively. A similar data acquisition system was used to determine the monochromatic incident photon to electric current conversion efficiency. Under full computer control, light from a 300 W xenon lamp (ILC Technology, USA) was focused through a Gemini-180 double monochromator (Jobin Yvon Ltd., UK) onto the photovoltaic cell to be tested. The monochromator was incremented through the visible spectrum to generate the IPCE($\lambda$), defined by IPCE($\lambda$) = $12400(J_{sc}/\lambda\varphi)$, where $\lambda$ is the wavelength, $J_{sc}$ is short-circuit photocurrent density (mA cm$^{-2}$), and $\varphi$ is the incident radiative flux (mW cm$^{-2}$). Photovoltaic performance was measured by using a metal mask with an aperture area of 0.12 cm$^2$. The measurments were preformend under bias light. The cross section of the device was measured by using a Zeiss Jemini FEG-SEM instrument at 5 kV with magnification of 250K×.

## ■ AUTHOR INFORMATION

### Corresponding Author

lioz.etgar@mail.huji.ac.il

### Notes

The authors declare no competing financial interest.

## ■ ACKNOWLEDGMENTS

The authors thank Carole Graetzel for fruitful discussions. This work was partially supported by EU FP7 project ENERGY-

261920 “ESCORT”. M.K.N. thanks the World Class University program, Photovoltaic Materials, Department of Material Chemistry, Korea University, Chungnam, 339-700, Korea, funded by the Ministry of Education, Science and Technology through the National Research Foundation of Korea (No. R31-2008-000-10035-0). FP7-NMP-2009 Project SANS under the contract No. NMP-246124, and ORION grant agreement number NMP-229036. The Research was partially supported by the King Abdullah University of Science and Technology (KAUST, Award No KUS- C1-015-21).

## REFERENCES

(1) Huynh, W. U.; Dittmer, J. J.; Alivisatos, A. P. *Science* **2002**, *295*, 2425.

(2) Gur, I.; Fromer, N. A.; Geier, M. L.; Alivisatos, A. P. *Science* **2005**, *310*, 462.

(3) Beek, W. J. E.; Wienk, M. M.; Janssen, R. A. J. *Adv. Funct. Mater.* **2006**, *16*, 1112.

(4) Luther, J. M.; Law, M.; Beard, M. C.; Song, Q.; Reese, M. O.; Ellingson, R. J.; Nozik, A. J. *Nano Lett.* **2008**, *8*, 3488.

(5) Ma, W.; Luther, J. M.; Zheng, H.; Wu, Y.; Alivisatos, A. P. *Nano Lett.* **2009**, *9*, 1699.

(6) Plass, R.; Pelet, S; Krueger, J.; Grätzel, M.; Bach, U. *J. Phys. Chem. B* **2002**, *106*, 7578.

(7) Sun, B.; Findikoglu, A. T.; Sykora, M.; Werder, D. J.; Klimov, V. I. *Nano Lett.* **2009**, *9*, 1235.

(8) Luther, J. M.; Law, M.; Song, Q.; Perkins, C. L.; Beard, M. C.; Nozik, A. J. *ACS Nano* **2008**, *2*, 271.

(9) Zhang, S.; Cyr, P. W.; McDonald, S. A.; Konstantatos, G.; Sargent, E. H. *Appl. Phys. Lett.* **2005**, *87*, 233101.

(10) Hyun, B.-R.; Zhong, Y.-W.; Bartnik, A. C.; Sun, L.; Abruña, H. D.; Wise, F. W.; Goodreau, J. D.; Matthews, J. R.; Leslie, T. M.; Borrelli, F. *ACS Nano* **2008**, *2*, 2206.

(11) Ratan, D.; Jiang, T.; Barkhouse, D. A.; Xihua, W.; Andras, G. P.-A.; Lukasz, B.; Larissa, L.; Sargent, E. H. *J. Am. Chem. Soc.* **2010**, *132*, 5952.

(12) Luther, J. M.; Gao, J.; Lloyd, M. T.; Semonin, O. E.; Beard, M. C.; Nozik, A. J. *Adv. Mater.* **2010**, *22*, 3704.

(13) Pattantyus-Abraham, A. G.; Kramer, I. J.; Barkhouse, A. R.; Wang, X.; Konstantatos, G.; Debnath, R.; Levina, L.; Raabe, I.; Nazeeruddin, M. K.; Gratzel, M.; Sargent, E. H. *ACS Nano* **2010**, *4*, 3374.

(14) Liu, H.; Tang, J.; Kramer, I. J.; Debnath, R.; Koleilat, G. I.; Wang, X.; Fisher, A.; Li, R.; Brzozowski, L.; Levina, L.; Sargent, E. H. *Adv. Mater.* **2011**, *23*, 3832.

(15) Gao, J.; Luther, J. M.; Semonin, O. E.; Ellingson, R. J.; Nozik, A. J.; Beard, M. C. *Nano Lett.* **2011**, *11*, 1002.

(16) Gao, J.; Perkins, C. L.; Luther, J. M.; Hanna, M. C.; Chen, H. Y.; Semonin, O. E.; Nozik, A. J.; Ellingson, R. J.; Beard, M. C. *Nano Lett.* **2011**, *11*, 3263.

(17) Barkhouse, D. A. R.; Debnath, R.; Kramer, I. J.; Zhitomirsky, D.; Pattantyus-Abraham, A. G.; Levina, L.; Etgar, L.; Grätzel, M.; Sargent, E. H. *Adv. Mater.* **2011**, *23*, 3134.

(18) Wang, X.; Koleilat, G. I.; Tang, J.; Liu, H.; Kramer, I. J.; Debnath, R.; Brzozowski, L.; Barkhouse, D. A. R.; Levina, L.; Hoogland, S.; Sargent, E. H. *Nature Photonics* **2011**, *5*, 480.

(19) Leschikies, K. S.; Beatty, T. J.; Kang, M. S.; Norris, D. J.; Aydil, E. S. *ACS Nano* **2009**, *3*, 3638.

(20) Etgar, L.; Zhang, W.; Gabriel, S.; Hickey, S. G.; Nazeeruddin, Md. K.; Eychmüller, A.; Liu, B.; Grätzel, M. *Adv. Mater.* **2012**, *24*, 2202.

(21) Etgar, L.; Moehl, T.; Tscharntke, S.; Hickey, S. G.; Eychmüller, A.; Grätzel, M. *ACS Nano* **2012**, *6*, 3092.

(22) Sambur, J. B.; Novet, T.; Parkinson, B. A. *Science* **2010**, *330*, 63.

(23) Semonin, O. F.; Luther, J. M.; Choi, S; Chen, H. Y.; Gao, J; Nozik, A. J.; Beard, M. C. *Science* **2011**, *334*, 1530.

(24) Kojima, A.; Ikegami, M.; Teshima, K.; Miyasaka, T. *Chem. Lett.* **2012**, *41*, 397.

(25) Covaliu, C. I.; Chioaru, L. C.; Craciun, L.; Oprea, O.; Jitaru, I. *Optoelectron. Adv. Mater.* **2011**, *5*, 1097.

(26) Kagan, C. R.; Mitzi, D. B.; Dimitrakopoulos, C. D. *Science* **1999**, *286*, 945.

(27) Mitzi, D. B.; Feild, C. A.; Schlesinger, Z.; Laibowitz, R. B. *J. Solid State Chem.* **1995**, *114*, 159.

(28) Kojima, A.; Teshima, K.; Shirai, Y.; Miyasaka, T. *J. Am. Chem. Soc.* **2009**, *131*, 6050.

(29) Im, J.-H.; Chung, J.; Kim, S.-J.; Park, N.-G. *Nanoscale Res. Lett.* **2012**, *7*, 353.

(30) Im, J.-H.; Lee, C.-R.; Lee, J.-W.; Park, S.-W.; Park, N.-G. *Nanoscale* **2011**, *3*, 4088.

(31) Kim, H.-S.; Lee, C.-R.; Im, J.-H.; Lee, K.-B.; Moehl, T.; Marchioro, A.; Moon, S.-J.; Humphry-Baker, R.; Yum, J.-H.; Moser, J. E.; Grätzel, M.; Park, N.-G. *Nat. Sci. Rep.* **2012**, *2*, 591.

(32) Chung, I.; Lee, B.; He, J.; Chang, R. P. H.; Kanatzidis, M. G. *Nature* **2012**, *485*, 486.

(33) Han, X.; Kuang, Q.; Jin, M.; Xie, Z.; Zheng, L. *J. Am. Chem. Soc.* **2009**, *131*, 3152.

(34) Moon, S. J.; Yum, J. H.; Humphry-Baker, R.; Karlsson, K. M.; Hagberg, D. P.; Marinado, T.; Hagfeldt, A.; Sun, L. C.; Grätzel, M.; Nazeeruddin, M. K. *J. Phys. Chem. C* **2009**, *113*, 16816.